JASN

J Am Soc Nephrol. 2017 Apr; 28(4): 1162–1174.
Published online 2016 Nov 11. doi: 10.1681/ASN.2015111266

PMCID: PMC5373441
PMID: 27837149

Chronic Hyperphosphatemia and Vascular Calcification Are Reduced by Stable Delivery of Soluble Klotho

Julia M. Hum,[*] Linda M. O'Bryan,[†] Arun K. Tatiparthi,[‡] Taryn A. Cass,[*] Erica L. Clinkenbeard,[*] Martin S. Cramer,[†] Manoj Bhaskaran,[§] Robert L. Johnson,[§] Jonathan M. Wilson,[‖] Rosamund C. Smith,[✉†] and Kenneth E. White[✉*]

[*]Department of Medical and Molecular Genetics, Division of Molecular Genetics and Gene Therapy, Indiana University School of Medicine, Indianapolis, Indiana;
[†]Biotechnology Discovery Research, Lilly Research Laboratories,
[§]Investigational Pathology, and
[‖]Tailored Therapeutics, Eli Lilly and Company, Indianapolis, Indiana; and
[‡]Lead Optimization Toxicology and Pharmacology, Covance Inc., Greenfield, Indiana
[✉]Corresponding author.
J.M.H. and L.M.O. contributed equally to this work.
Correspondence: Dr. Rosamund C. Smith, Biotechnology Discovery Research, Eli Lilly and Company, Lilly Corporate Center, Indianapolis, IN 46285, or Dr. Kenneth E. White, Indiana University School of Medicine, Department of Medical and Molecular Genetics, 975 West Walnut Street, IB130, Indianapolis, IN 46202. Email: smith_rosamund_c@lilly.com or kenewhit@iupui.edu

Received 2015 Nov 24; Accepted 2016 Oct 1.

Abstract

Go to:

αKlotho (αKL) regulates mineral metabolism, and diseases associated with αKL deficiency are characterized by hyperphosphatemia and vascular calcification (VC). αKL is expressed as a membrane-bound protein (mKL) and recognized as the coreceptor for fibroblast growth factor-23 (FGF23) and a circulating soluble form (cKL) created by endoproteolytic cleavage of mKL. The functions of cKL with regard to phosphate metabolism are unclear. We tested the ability of cKL to regulate pathways and phenotypes associated with hyperphosphatemia in a mouse model of CKD-mineral bone disorder and α*KL*-null mice. Stable delivery of adeno-associated virus (AAV) expressing cKL to diabetic endothelial nitric oxide synthase–deficient mice or α*KL*-null mice reduced serum phosphate levels. Acute injection of recombinant cKL downregulated the renal sodium-phosphate cotransporter Npt2a in α*KL*-null mice supporting direct actions of cKL in the absence of mKL. α*KL*-null mice with sustained AAV-cKL expression had a 74%–78% reduction in aorta mineral content and a 72%–77% reduction in mineral volume compared with control-treated counterparts ($P<0.01$). Treatment of UMR-106 osteoblastic cells with cKL + FGF23 increased the phosphorylation of extracellular signal–regulated kinase 1/2 and induced Fgf23 expression. CRISPR/Cas9-mediated deletion of fibroblast growth factor receptor 1 (FGFR1) or pretreatment with inhibitors of mitogen–activated kinase kinase 1 or FGFR ablated these responses. In summary, sustained cKL treatment reduced hyperphosphatemia in a mouse model of CKD-mineral bone disorder, and it reduced hyperphosphatemia and prevented VC in mice without endogenous αKL. Furthermore, cKL stimulated Fgf23 in an FGFR1-dependent manner in bone cells. Collectively, these findings indicate that cKL has mKL-independent activity and suggest the potential for enhancing cKL activity in diseases of hyperphosphatemia with associated VC.

Keywords: FGF23, hyperphosphatemia, alpha-klotho, osteocyte, bone, db/db-eNOS

CKD-mineral bone disorder (CKD-MBD) is associated with increased serum fibroblast growth factor-23 (FGF23), hyperphosphatemia, and vascular calcification (VC), and more recently, it has been linked to αKlotho (αKL) deficiency.[1–3] In CKD-MBD, patient hyperphosphatemia is correlated with increased VC and risk of death.[4,5] Therefore, a primary goal in the management of CKD-MBD is the control of systemic phosphate accumulation as the kidneys fail. However, the current approaches of reducing dietary consumption of phosphate in combination with intestinal phosphate binders are only partially effective.[6–8] αKL is a key regulator of mineral metabolism, and in concert with the bone–derived hormone FGF23, maintains phosphate and vitamin D homeostasis through a bone-kidney endocrine axis.[9–14] Indeed, the importance of the interactions between these factors is highlighted by the findings that loss of function mutations in α*KL*[15] and *FGF23*[16–19] lead to the Mendelian disorder hyperphosphatemic familial tumoral calcinosis. In the reciprocal setting, gain of function mutations in *FGF23* result in increased blood FGF23 and autosomal dominant hypophosphatemic rickets.[20] Importantly, the α*KL*- and *Fgf23*-knockout mice are hyperphosphatemic and have severe VC.[21–25] Mechanistic and genetic experiments in these models showed that the elevated blood phosphate through loss of α*KL* or *Fgf23* is due to increased renal reabsorption of phosphate as well as increased 1,25D, leading to elevated intestinal phosphate absorption.[22,23,25] The db/db-endothelial nitric oxide synthase (eNOS)$^{-/-}$ mouse model of diabetic nephropathy (DN) mimics the human disease in several regards. With the loss of activity of the leptin receptor and disruption of eNOS, these animals develop highly elevated blood glucose and progressive renal damage, including glomerular and interstitial fibrosis.[26,27] Because DN is now the leading cause of CKD-MBD,[28,29] understanding the nature of this syndrome is important for identifying potential novel management approaches. The α*KL*- and *Fgf23*-knockout mice share key phenotypes associated with CKD-MBD, including uncontrollably elevated serum phosphate as well as ectopic calcification and VC.[21–25] Indeed, these animals have been important in determining the mechanisms underlying the relationships between *α*KL and FGF23 in renal failure, including downregulation of *α*KL in the kidney leading to FGF23 resistance and the concept that gradually increasing FGF23 reduces 1,25D, resulting in hyperparathyroidism.[12,23] Therefore, these rare and common syndromes and their orthologous animal models underscore the importance of *α*KL and FGF23 to maintain normal phosphate and 1,25D metabolism.

*α*KL is predominantly expressed in the kidney and parathyroid glands but can also be found in blood, urine, and cerebrospinal fluid.[22,30] Two main forms of *α*KL exist; a full–length transmembrane protein (mKL; 135 kD) and a circulating soluble form (cKL; 110 kD). The cKL polypeptide is generated through activity of the ADAM10/17 and BACE proteases near the mKL extracellular transmembrane region, which liberates the cKL polypeptide comprised of the KL1 and KL2 extracellular domains.[31] FGF23 initiates signaling in the kidney and parathyroids through a coordinated assembly of mKL coreceptor complexed with fibroblast growth factor receptors (FGFRs), leading to activation of the MAPK cascade.[21,32–35] A previous study showed that cKL injection caused phosphaturia *in vivo*[35]; however, relatively little is known about the specificity or bioactivity of cKL in regard to its direct interactions with pathways controlling phosphate and vitamin D metabolism. The mKL form has been stably overexpressed to examine its role in a number of disease states, including hypertension and renal damage,[37,38] although this approach presumably results in production of cKL as well. Thus, a full understanding of the requirements for the presence of mKL for cKL bioactivity is needed. Furthermore, determining whether cKL is independent of mKL for its biologic actions in conditions of hyperphosphatemia expands the potential to explore cKL-mediated events as targets for therapeutic intervention in situations of endogenous *α*KL insufficiency.

We previously showed that stable delivery of cKL to wild-type (WT) mice resulted in hypophosphatemia and increased FGF23 expression.[39] Furthermore, these manifestations in the mouse phenocopied those of a patient with a chromosome 9:13 genomic translocation proximal to the α*KL* gene, resulting in elevated serum cKL.[40] Collectively, these studies support that cKL may play a role in phosphate handling.

Therefore, this study sought to test the mechanisms underlying cKL actions in the db/db-eNOS$^{-/-}$ model and with the loss of αKL and hyperphosphatemia in α*KL*-null mice. In this regard, cKL, when stably delivered, was associated with a reduction in serum phosphate in both models and prevented aortic calcification in the α*KL*-null animals. Additionally, cKL downregulated Npt2a expression in the kidney and stimulated FGFR1-dependent production of FGF23 in bone cells. Taken together, these findings support the concept that targeting cKL-mediated pathways may ameliorate defects in mineral metabolism associated with diseases of hyperphosphatemia. Thus, our results have important implications for managing cardiovascular and endocrine outcomes caused by aberrant phosphate handling.

Results

Go to:

cKL Rescues Hyperphosphatemia in a Model of DN

DN is the most common form of CKD-MBD. The gene *Nos3* encoding eNOS is responsible for the nephropathic changes in mouse models of types 1 and 2 diabetes.[41–43] The db/db-eNOS$^{-/-}$ model serves as a useful tool in studying therapeutic interventions for CKD-MBD phenotypes evident in DN.[26,27] On histologic characterization of these mice, it was confirmed that the db/db-eNOS$^{-/-}$ animals exhibited a prominent presence of tubular protein (arrowheads and inset in Figure 1A, iv) and dilated tubules (arrows in Figure 1A, iv) with undulation of the subcapsular cortex due to underlying fibrosis. Noticeable mesangial matrix deposition obliterating normal capillary loops and cellularity in the glomeruli (arrows and inset in Figure 1A, v) was observed in db/db-eNOS$^{-/-}$ mice compared with control lean mice (Figure 1A, i–iii). The db/db-eNOS$^{-/-}$ mice also had marked interstitial fibrosis (stars in Figure 1A, vi) and prominent glomerular fibrosis (arrows and inset in Figure 1A, vi) with occasional glomerular sclerosis (arrowhead in Figure 1A, vi), consistent with findings from the human syndrome.[44,45] No change in renal histopathology was observed in adeno-associated virus 2/8 (AAV)-cKL–treated mice (data not shown).

To test sustained delivery of cKL on the accompanying hyperphosphatemia exhibited by db/db-eNOS$^{-/-}$ mice, cKL was delivered *via* AAV-cKL under the regulation of a hepatic-specific promoter or control AAV-LacZ to 13- to 17-week-old db/db-eNOS$^{-/-}$ mice *via* retro-orbital injection for 6 weeks. AAV-cKL delivery did not affect body weight in the db/db-eNOS$^{-/-}$ mice compared with AAV-LacZ, but db/db-eNOS$^{-/-}$ mice were significantly heavier than control lean mice (Figure 1B) ($P<0.01$). Blood glucose was elevated in female db/db-eNOS$^{-/-}$ mice compared with lean controls at baseline (Figure 1C) ($P<0.01$). Through our observations of this CKD-MBD model, males shared the majority of disease phenotypes with females but were prone to earlier death. Indeed, the analysis of the interim time points produced significant results in males; however, at the final 6-week time point, the AAV-LacZ males were reduced to $n=2$ and are, thus, included for relative comparisons. Urine albumin-to-creatinine ratio (ACR) was elevated compared with that in lean control mice but unchanged across db/db-eNOS$^{-/-}$ groups (Figure 1D) ($P<0.01$). With AAV-cKL administration, serum cKL levels were robustly increased in male and female db/db-eNOS$^{-/-}$ mice at 6 weeks (Figure 1F) ($P<0.01$ versus female; $P<0.05$ versus male). Consistent with previous results, serum intact FGF23 was elevated with delivery of AAV-cKL to male and female db/db-eNOS$^{-/-}$ mice by 4 weeks of treatment (Figure 1G) ($P<0.05$). Whereas improvements in markers of renal function were not observed with AAV-cKL treatment, hyperphosphatemia was notably corrected by AAV-cKL in female db/db-eNOS$^{-/-}$ mice (Figure 1H) ($P<0.05$), with minimal effects on serum calcium (Figure 1E) ($P<0.05$).

Effects of cKL on Phosphate Metabolism *In Vivo* in αKL-Null Background

Although the db/db-eNOS$^{-/-}$ model parallels patients with CKD-MBD with regards to kidney function and hyperphosphatemia, these mice do not develop the VC characteristic of advanced stage CKD-MBD.[27] Therefore, AAV-cKL was administered to 4-week-old WT and α*KL*-null mice that display severe VC and hyperphosphatemia.[22,23] Delivery of AAV-cKL was confirmed by liver immunohistochemistry (IHC)

staining for αKL, which showed robust positive staining in the cells surrounding the hepatic portal venules (Figure 2A). Consistent with these analyses, liver mRNA expression of *α*KL was highly elevated in the AAV-cKL–treated mice (40- to 60,000-fold increase versus the vehicle and AAV-LacZ controls) (Figure 2B). Additionally, the general histology of the liver was normal across genotypes and treatments (not shown).

Serum biochemistries were examined at baseline (4 weeks of age before AAV) and after 4 weeks of treatment. After AAV-cKL delivery, serum phosphate was significantly reduced in WT mice (Figure 2C) ($P<0.01$), whereas vehicle and AAV-LacZ treatment groups maintained normal phosphate in accordance with previous results.[38] Regardless of treatment, α*KL*-null mice exhibited significantly elevated serum phosphate at baseline and euthanasia compared with both WT vehicle and WT AAV-LacZ treatment groups (Figure 2C) ($P<0.001$ and $P<0.01$, respectively). After AAV-cKL treatment, however, α*KL*-null mice had reduced serum phosphate compared with α*KL*-null vehicle and AAV-LacZ–treated groups (Figure 2C) ($P<0.01$), similar to the db/db-eNOS$^{-/-}$ mice. The α*KL*-null mice administered AAV-cKL exhibited slightly elevated calcium levels after 4 weeks of treatment versus WT-cKL but not versus α*KL*–null control groups (Figure 2D) ($P<0.05$).

In addition to mineral ion alterations, hyperparathyroidism was induced in WT mice treated with AAV-cKL (Figure 2E) ($P<0.05$); however, α*KL*-null mice remained hypoparathyroid, regardless of treatment (Figure 2E) ($P<0.05$ versus WT respective treatment). α*KL*-null mice had elevated FGF23 in the basal condition (Figure 2F) ($P<0.01$) largely due to loss of the appropriate negative feedback loops for phosphate and 1,25D between kidney and bone to suppress FGF23 production.[21] Serum FGF23 levels were increased in the WT AAV-cKL group (Figure 2F, inset) ($P<0.01$), consistent with previous results. AAV-cKL further induced serum FGF23 in the *α*KL-null mice compared with both vehicle and AAV-LacZ–treated cohorts (Figure 2F) ($P<0.01$).

Renal Activity of cKL

We next examined serum 1,25D concentrations in the AAV-cKL– and control–treated groups and found that, compared with controls, 1,25D in WT AAV-cKL was suppressed (Figure 3A) ($P<0.01$), whereas in α*KL*-null mice, control-treated groups had elevated 1,25D (Figure 3A) ($P<0.01$), and α*KL*–null AAV-cKL–treated mice had normalized 1,25D compared with the respective genotype controls (Figure 3A) ($P<0.05$). Additionally, expression of renal enzymes regulating 1,25D was altered by AAV-cKL delivery. In both WT and α*KL*-null mice, a reduction in 1*α*-OHase (*Cyp27b1*) expression occurred with AAV-cKL treatment (Figure 3B) ($P<0.05$). Renal expression of 24-OHase (*Cyp24a1*) was increased in WT mice delivered AAV-cKL (Figure 3C) ($P<0.05$), whereas α*KL*-null mice treated with AAV-cKL had a trend for increased 24-OHase, but it was not statistically significant (Figure 3C). As shown above, AAV-cKL treatment reduced serum phosphate *in vivo* in α*KL*-null mice. The primary kidney sodium-phosphate cotransporter, Npt2a, is highly upregulated in *α*KL-null mice,[35] leading to increased renal phosphate reabsorption. Therefore, cKL's ability to modulate Npt2a expression in the absence of mKL was next tested in short-term experiments to avoid long–term endocrine compensatory effects. In this regard, recombinant cKL (1 *μ*g/g body wt), FGF23 (1 *μ*g/g body wt), or vehicle was injected intravenously into α*KL*-null mice. cKL delivery was confirmed by Klotho assay (vehicle and FGF23–treated mice had undetectable levels of Klotho, whereas cKL-treated mice ranged from 214 to 526 ng/ml). The mice receiving vehicle or FGF23 had readily detectable Npt2a protein on IHC analysis (Figure 3, D and E). In contrast, after 1-hour injection with cKL, quantitation of Npt2a protein showed a 75% reduction versus vehicle-injected mice (Figure 3, F and G) ($P<0.01$). These results support that cKL is capable of controlling 1,25D as well as Npt2a expression in the absence of mKL.

cKL Effects on Aortic Calcification

As determined by microcomputed tomography (*μ*CT) analysis, some α*KL*-null mice showed slight aortic

calcification at the baseline pretreatment age of 4 weeks (Figure 4A), whereas WT mice had no detectable signs of aortic defects at any time point (not shown). Four weeks later at 8 weeks of age, vehicle and AAV-LacZ–treated α*KL*–null mice had dramatic increases in aortic calcification (Figure 4, B and C). In contrast, the α*KL*-null mice receiving AAV-cKL had a 78% reduction in total aortic mineral content compared with the AAV-LacZ group and a 74% reduction compared with vehicle (Figure 4E) ($P<0.01$). Aortic mineral volumes were also 72% and 77% lower in α*KL*-null mice treated with AAV-cKL compared with vehicle or AAV-LacZ, respectively (Figure 4F) ($P<0.01$). Segmental analysis of the ascending, arch, and descending aortas confirmed the marked reduction in mineral content and volume (Supplemental Figure 1).

In parallel with μCT analysis, histology of the isolated aortas was performed on longitudinal sections stained with hematoxylin and eosin (H&E). Compared with respective WT controls (Figure 4G), vehicle or AAV-LacZ–treated α*KL*–null mice had multifocal disruption or expansion of the elastic lamina (arrows in Figure 4H). In contrast, <50% of such lesions in cKL-treated mice showed mineralized patches.

Mechanisms of cKL Activity in Bone

To test the mechanisms for the increased serum FGF23 after AAV-cKL delivery, femoral FGF23 RNA expression was examined. Compared with controls, WT-cKL mice exhibited a 230-fold elevation of bone FGF23 mRNA (Figure 5A) ($P<0.01$). α*KL*-null mice receiving vehicle or AAV-LacZ displayed basally elevated FGF23 mRNA compared with WT controls, and AAV-cKL treatment produced an additional increase (Figure 5A) ($P<0.01$). These changes paralleled the serum FGF23 concentrations for each WT and α*KL*-null control and AAV-cKL–treated group (Figure 2D).

Typically, FGF23 is suppressed by reductions in serum phosphate; thus, the mechanisms underlying the observed increases in serum and bone FGF23 during AAV-cKL administration were unclear. Extracellular portions of mKL have been shown to assemble with FGFR1 before FGF23 binding and complex activation.[32] Therefore, we next tested *in vitro* whether cKL activated FGFR-dependent pathways and whether FGF23 was required for cKL signaling in the context of bone. The UMR-106 osteoblastic cell line expressed readily detectable FGFR1 protein[46]; thus, this line was treated with the positive control FGF8 as well as cKL and FGF23 either alone or in combination. Early growth response-1 (EGR1) mRNA production was assessed as a recognized marker of FGFR bioactivity.[21,47] The administration of cKL or FGF23 alone did not induce EGR1 expression (Figure 5B). FGF8 stimulated EGR1 mRNA (Figure 5B) ($P<0.001$), and EGR1 mRNA was dose dependently increased after escalating doses of cKL + FGF23, including a 40-fold increase at the highest dose (Figure 5B) ($P<0.001$). Compared with cKL and FGF23 alone, FGF23 mRNA also increased 9.6-fold in UMR-106 cells after cKL + FGF23 delivery (Figure 5C) ($P<0.01$), supporting direct cKL activity on bone cells. Consistent with FGFR-dependent activity, immunoblots showed that cKL + FGF23 treatment increased p–extracellular signal–regulated kinase 1/2 (p-ERK1/2) (Figure 5D, inset), whereas MEK (U0126) and FGFR (PD173074) inhibitors ablated the EGR1 mRNA increase (Figure 5D) ($P<0.001$) and p-ERK1/2 responses (Figure 5D, inset).

To isolate the molecular mechanisms associated with cKL activity, a novel UMR-106 line was generated *via* clustered regularly interspaced short palindromic repeats (CRISPR)–mediated deletion of FGFR1. FGFR1 protein was readily detectable in the parent cell line (UMR), and receptor deletion was assured by immunoblot (Figure 5E, CRISPR cell line in inset). Compared with UMR cells, the elevation of FGF23 mRNA in response to cKL + FGF23 was completely ablated in the CRISPR line (Figure 5E) ($P<0.001$ versus UMR cKL + FGF23). Comparably, EGR1 expression was also markedly blunted in response to FGF2, FGF8, and cKL + FGF23 (Figure 5F) ($P<0.05$ versus UMR respective treatment). Furthermore, with FGFR1 deletion, an agonist antibody for FGFR1c[48] did not increase FGF23 mRNA production compared with parent UMR cells (Figure 5G). Taken together, these findings support that cKL mediates FGFR-dependent signaling in bone cells, that the presence of FGF23 facilitates this activity, and that the delivery

of cKL to bone *in vivo* is a more powerful stimulator of FGF23 than reduced serum phosphate is a repressor.

In sum, these findings show that cKL reduces serum phosphate and ameliorates hyperphosphatemia-associated VC in the absence of mKL. Additionally, cKL acts in bone through FGFR1 to control FGF23 expression. Thus, enhancing cKL activity or its downstream pathways may be useful for controlling important aspects of altered phosphate metabolism in disease.

Discussion

Go to:

In genetic and acquired diseases involving hyperphosphatemia, including CKD-MBD, the inability of the kidney to clear excess phosphate causes severe endocrine disturbances as well as leads to calcification of the vasculature.[5,49,50] The syndrome of DN is the leading cause of CKD-MBD and thus, of primary concern clinically. *α*KL expression levels are decreased in kidneys of patients with early DN.[28,29] Consistent with earlier reports,[26,27] we found that the db/db-eNOS$^{-/-}$ mouse model had marked kidney fibrosis and increased ACR as well as hyperphosphatemia. Delivery of AAV-cKL increased serum cKL and FGF23 and reduced serum phosphate in these animals, supporting that sustaining cKL concentrations can overcome diminished renal function to improve mineral metabolism. Because this mouse line does not develop VC, we next tested AAV-cKL in the α*KL*-null mice. It is known that this model exhibits severe hyperphosphatemia and VC, similar to that in patients with hyperphosphatemic familial tumoral calcinosis and loss of function mutations in α*KL* and *FGF23*.[11,15–17] Previous studies testing a variety of interventions showed effects on lessening VCs in α*KL*-null mice but failed to significantly correct the hyperphosphatemia. In this regard, an experimental approach of treating α*KL*-null mice with NH_4Cl reduced VC by preventing the osteoinduction of vascular smooth muscle cells through a reduction in TGF*β*1 and inhibition of NFAT5–dependent osteochondrogenic signaling.[51] Similarly, although not affecting serum phosphate or FGF23 concentrations, acetazolamide partially reversed aortic calcification in α*KL*-null mice through incompletely defined mechanisms.[51] Thus, whether these methods target the vasculature as well as pathways that control phosphate handling remains unclear.

Interestingly, one report showed that overexpression of the mKL isoform reduced aortic calcification in α*KL*-null mice[23]; however, whether this was due to increased presence of circulating cKL is unclear. We previously showed that cKL reduced serum phosphate concentrations when AAV-cKL was delivered stably *in vivo* to WT mice.[39] These animals exhibited hypophosphatemia with elevated FGF23, similar to a patient with an α*KL* gene translocation, which resulted in markedly elevated plasma cKL.[40] In the animal studies, cKL treatment likely reduced serum phosphate by elevating FGF23 mRNA and protein, leading to the appropriate renal gene responses, including decreased Npt2a and *Cyp27b1* expression as well as increased *Cyp24a1* in the presence of all endogenous *α*KL isoforms.[39] In the WT genetic background, however, it was difficult to determine the contributions of the individual *α*KL isoforms to elicit these phenotypes and whether the actions of cKL required mKL. To further dissect the actions of the αKL forms, cKL was delivered to α*KL*-null mice. With the loss of all *α*KL isoforms, α*KL*-null mice can no longer mediate efficient FGF23-dependent signaling in target tissues, resulting in elevated serum phosphate and 1,25D. Providing only the cKL form in a sustained manner created the ability to test this factor's activity and pharmacologic potential in the absence of mKL in an environment of hyperphosphatemia. Similar to mice conditionally lacking parathyroid *α*KL expression, α*KL*-null mice may maintain low parathyroid hormone (PTH) levels by using an *α*KL–independent calcineurin–mediated FGF23 signaling pathway to suppress the secretion of PTH,[53] which could occur, in part, with the known negative feedback loop between 1,25D and PTH. Indeed, we showed that cKL, likely through the elevated FGF23, reduced serum 1,25D in WT mice, leading to hyperparathyroidism. In α*KL*-null mice, 1,25D was also normalized, however potentially not to a level to fully correct PTH. In the future, studies using an inducible cKL model could provide further insight into the dosing required for tissue–specific cKL effects.

This study shows that stable delivery of cKL to db/db-eNOS$^{-/-}$ and α*KL*-null mice reduced the prevailing hyperphosphatemia as well as ameliorated the associated VC in α*KL*-null mice. These findings raise the possibility that targeting cKL-mediated pathways may alleviate pathogenic hallmarks of hyperphosphatemic disease. It remains unclear, however, whether cKL can substitute for mKL at physiologic levels, because our findings may potentially reflect a pharmacologic action of elevated cKL in the setting of increased FGF23 in α*KL*-null mice or during CKD. Although they have provided tremendous insight into phosphate handling, α*KL*-null mice are not a model of progressive renal failure. However, CKD-MBD has been recognized as a state of renal *α*KL deficiency,[54,55] where *α*KL expression was shown to be rapidly downregulated early in disease, leading to alterations in phosphate metabolism.[56] Underscoring the importance of these pathogenic events is the finding that cardiovascular disease resulting from excessive VC is a common cause of death in patients on dialysis.[57–59] Although other aspects of CKD-MBD, such as the progressive renal failure as evidenced by increasing ACR values as well as disturbed glucose handling, were not improved, the reduction in serum phosphate was significant. These results support the concept that cKL likely affects mineral metabolism through interactions with FGF23 more effectively than other manifestations of DN.

The ability of cKL repletion to significantly lower serum phosphate in the α*KL*-null mouse suggested that cKL induced effects on phosphate handling genes in isolation from mKL. This was shown by cKL's ability to reduce serum 1,25D by decreasing the renal 1*α*-OHase expression. To test the direct activity of cKL on the kidney, acute injections of cKL were performed, which reduced Npt2a protein expression. Consistent with these results, it was previously shown that cKL may directly interact with Npt2a to decrease its expression on the proximal tubule apical membrane, resulting in a suppression of phosphate reuptake.[36] Although serum phosphate levels in the α*KL*-null mice were not restored to WT levels with AAV-cKL treatment, this effect may significantly contribute to the observed reduction in aortic calcification. However, direct effects of recombinant cKL on vasculature have been previously reported[23]; thus, at this time, we cannot differentiate direct versus indirect actions for cKL. Unlike the increase in PTH caused by cKL treatment in WT mice, which may occur through FGF23-mediated suppression of 1,25D production,[39] PTH status in α*KL*-null mice remained suppressed after cKL delivery. We found that the α*KL*-null mice treated with AAV-cKL had serum intact FGF23 and bone FGF23 mRNA concentrations significantly above the prevailing elevated FGF23 levels in control α*KL*–null mice.

Sustained delivery of cKL was capable of eliciting increased FGF23 expression *in vivo* in the absence of mKL as well as the presence of FGF23 in the osteoblastic cell line UMR-106. Consistent with these findings, the α*KL* translocation patient with elevated serum cKL showed markedly increased FGF23 in the face of hypophosphatemia, typically a strong suppressor of FGF23 production.[40] Similarly, we showed that AAV-cKL stimulated FGF23 in serum and whole bone in α*KL*-null mice to levels that were above the already elevated baseline seen in these mice.[39] These results show that cKL may function independently of phosphate-sensing mechanisms to increase FGF23 at pharmacologic doses. Through *in vitro* studies in UMR-106 bone cells, we showed that cKL in combination with FGF23 increased FGF23 expression. Although other FGFRs cannot be ruled out, FGFR1 signaling was required for the overwhelming majority of this effect. Indeed, either pharmacologic inhibitors of MEK and FGFR signaling or genetic deletion of FGFR1 through CRISPR/Cas targeting ablated this response. These results are corroborated with other *in vitro* studies, including the demonstration that FGF23 promoter activity could be stimulated with FGFR1 agonists and was inhibited by dominant negative FGFR1 as well as PLC and MAPK inhibitors.[60] Our results also parallel findings that FGF23 expression was increased in calvaria-derived osteoblasts after treatment with a specific FGFR1–stimulating antibody.[61] Similarly, to test the role of FGFR1 and its influence on FGF23, this receptor was previously deleted from late osteoblasts/osteocytes *in vivo* using the Dentin matrix protein 1-cre. This cross resulted in mice with reduced serum intact FGF23 concentrations.[60] Furthermore, genetic findings showed that patients with osteoglophonic dysplasia due to FGFR1 gain of

function mutations had elevated FGF23 and hypophosphatemia.[82] α*KL* is primarily expressed in kidney; therefore, whether cKL acts under normal circumstances to directly communicate changes in renal FGF23 activity or serum phosphate concentrations to bone remains to be determined.

In summary, extended delivery of cKL was associated with decreased serum phosphate in both a model of DN and an α*KL*-null background along with a reduction in aortic calcification. Additionally, we identified other phenotypes in the α*KL*-null mice which cKL did not appear to target, including PTH production. Consistent with the actions of cKL on bone *in vivo*, cKL induced FGF23 in osteoblastic cells *in vitro* in an FGFR1-dependent fashion. These collective actions of cKL occur in the absence of mKL; thus, cKL does not require the presence of mKL for influencing important aspects of phosphate balance. Taken together, our findings support the potential for enhancing cKL activity or its downstream pathways for controlling important aspects of altered phosphate metabolism in disease.

Concise Methods

Go to:

Animal Studies

Animal studies were performed according to the Institutional Animal Care and Use Committee for Indiana University and the internal review board at Eli Lilly and Company (Indianapolis, IN), and they comply with the National Institutes of Health guidelines for the use of animals. AAV-cKL, AAV-LacZ, or vehicle (PBS) was delivered to 4-week-old WT or αKL-null mice[22] or 13- to 17-week-old db/dm (lean control) or db/db-eNOS$^{-/-}$ mice (Taconic Laboratories) *via* retro-orbital injection as previously described at 1×10^{11} genomic copies per mouse.[39] αKL-null mice received one half of this dose due to being, on average, 50% body size. Body weights and interim bleeds were taken at indicated times. For acute (1-hour) studies, α*KL*-null mice were intravenously injected with vehicle (PBS) or 1 μg/g body wt recombinant cKL or FGF23 and euthanized after 1 hour. All mice were euthanized by CO_2 inhalation and then, cervical dislocation.

Recombinant cKL and FGF23 and AAV-cKL Production and Delivery

The cDNA-encoding residues 35–983 of the cKL with a CD33 N–terminal signal sequence or β-galactosidase gene cassette (LacZ) as a control were packaged into a recombinant hybrid AAV (RegenX Biosciences). *In vivo* expression was driven by a liver–specific thyroxine binding globulin promoter. Recombinant cKL (mouse), FGF23 (human), and FGF8 (human) were obtained from R&D Systems.

μCT Analyses

μCT images were acquired with GE eXplore Locus RS *In Vivo* and GE eXplore Locus SP *Ex Vivo* Computed Tomography Scanners (TriFoil Imaging, Northridge, CA). Each mouse carcass was placed into a polypropylene tube and mounted on the Locus RS Scanner Bed along with a Hounsfield unit calibration phantom. Images were acquired using x-ray source parameters of 80 kVp and 450 μA along with a 1.8-mm-thick Al filter. A region covering the upper thorax to the sacrum was scanned for each mouse carcass. ImageJ software (National Institutes of Health, Bethesda, MD) was used to analyze the aorta region datasets. The aorta analysis included creating manual regions of interest of the aorta starting from the aortic arch to the abdominal aortic bifurcation. The aorta has the same x-ray attenuation as surrounding soft tissue; thus, the scapula and the sacral vertebrae were used to locate the aortic arch and abdominal aortic bifurcation, respectively.

Aorta Histology

After μCT, the aorta was removed and stored in 70% ethanol before being embedded in paraffin; 5-μm sections were prepared and stained with H&E or von Kossa by routine methods. Slides were evaluated for

histopathologic changes and von Kossa–positive mineral content by a board–certified veterinary pathologist (R.L.J.).

Histology

For liver histology, after necropsy, a lobe of liver was stored in 4% PFA before being embedded in paraffin; 5-μm histologic sections were stained with H&E before evaluation by an American College of Veterinary Pathologists–certified pathologist. Kidneys from the db/dm (lean control) or db/db-eNOS$^{-/-}$ mice were removed at euthanasia and fixed for at least 24 hours in 10% neutral buffered formalin. Tissues were trimmed, routinely processed, embedded in paraffin, sectioned, and then, stained with H&E, Masson trichrome, or periodic acid–Schiff stain. Histopathologic evaluation of these slides was conducted using an internally established grading system.

Serum and Urine Biochemistries

Standard calcium and inorganic phosphorous reagent kits were used for serum measurements in a Hitachi Analyzer (Roche Diagnostics). Serum Klotho was measured as previously described.[39] Serum FGF23 was tested using an Intact FGF23 ELISA (Kainos Laboratories). PTH was measured using a mouse–specific PTH ELISA (Immutopics International). Serum 1,25D was measured using an enzyme immunoassay (Immunodiagnostic Systems). Blood glucose measurements in the lean controls and db/db-eNOS$^{-/-}$-null mice were performed by using a Roche Aviva Accu-Check Glucometer. Whole blood was collected from a tail stick at times stated. Urine ACR was obtained through a spot urine collection over a 2- to 3-hour period and analyzed as previously described.[63]

Cell Culture and *In Vitro* Functional Assays

UMR-106 cells (ATCC) were cultured in DMEM/F-12 (Invitrogen) supplemented with 10% FBS (Hyclone), 1 mM sodium pyruvate, 25 mM L-glutamine, and 25 mM penicillin-streptomycin (Sigma-Aldrich) at 37°C and 5% CO_2. Cells were plated at 1.0×10^5 per well in a 12-well plate and treated with increasing doses of cKL (1, 10, and 30 nM) and FGF23 (4, 40, and 115 nM) either alone or in combination with each respective higher cKL and FGF23 dose or FGF8 (100 ng/ml) overnight before RNA extraction. Cells were administered MEK (10 μM; U0126; R&D Systems) or FGFR (80 μM; PD173074; R&D Systems) inhibitors for 1 hour before cKL and FGF23 exposure; cells were also treated with IMC-A1 FGFR1 agonist antibody (0.01 mg/ml)[47] for 48 hours before RNA extraction.

RNA Isolation and Quantitative PCR

Femur, kidney, and liver total RNA was harvested using Trizol Reagent (Life Technologies), and RNA from UMR-106 cells was isolated from cellular lysates using the RNeasy Kit (Qiagen, Inc.). RNA samples were tested by quantitative PCR with primers specific for mouse or rat *Fgf23*, *Egr1*, *Klotho*, *1α-OHase* (*Cyp27b1*), *24-OHase* (*Cyp24a1*), and internal control β-*actin* as previously described.[64] The TaqMan One-Step RT-PCR Kit (Life Technologies) was used to perform quantitative PCR, and data were collected using the 7500 Real Time PCR System and software (Life Technologies) and then, analyzed using the $2^{-\Delta\Delta CT}$ method.[65]

Immunoblotting

UMR-106 cells were lysed with 75 μl lysis buffer (Cell Signaling Technologies). Cell lysate protein concentrations were determined with the Better Bradford Kit (Thermo-Fisher Scientific) according to the manufacturer's instructions. Western blot analysis was performed with 30 μg cellular lysates. The blots were incubated with primary antibodies for anti–p-ERK1/2 (Cell Signaling Technologies) and antitotal

extracellular signal–regulated kinase (Promega) at 1:1000 or anti-FGFR1 (Sigma-Aldrich) at 1:400 and then, incubated with anti–rabbit IgG-GRP antibody at 1:5000 (Bio-Rad, Inc.). Blots were stripped using SDS-glycine and reprobed with 1:10,000 anti–β-actin-HRP (A3854; Sigma-Aldrich). Detection was performed using the ECL Plus Western Blotting Detection Reagents (Amersham-GE Healthcare) and X-Omat Film (Eastman-Kodak Co.).

IHC

Kidneys from α*KL*-null mice in the 1-hour study and livers from WT and α*KL*-null mice in the 4-week study were harvested after necropsy, fixed with 4% paraformaldehyde, and mounted in OCT (Sakura Finetek, Torrance, CA), and a standard microtome was used to prepare 7-μm sections. Kidney sections were treated with pepsin (Biocare Medical, Concord, CA) for antigen retrieval and then, an antibody to mouse Npt2a[66] followed by incubation with fluorescent secondary antibody (anti–rabbit IgG-Alexa Fluor; Invitrogen). Immunofluorescence signal amplification was performed using the Tyramide Signal Amplification Systems Kit according to the manufacturer's directions (Perkin Elmer, Waltham, MA). All slides were sealed with mounting reagent containing DAPI to stain nuclei (Vector Laboratories, Burlingame, CA). Imaging was performed using a Leica DM5000B Fluorescent Microscope (Leica Microsystems, Inc., Bannockburn, IL), and SPOT camera and computer program (RTKE Diagnostic Instruments, Inc., Sterling Heights, MI). A minimum of three to four animals per time point and eight to 12 sections per animal were examined for each primary antibody set. Quantification of Npt2a staining was performed using ImageJ software. Liver sections from WT and α*KL*-null mice delivered vehicle, AAV-LacZ, or AAV-cKL were treated with pepsin (Biocare Medical, Concord, CA) for antigen retrieval and then, an mAb to αKL (TransGenic, Kobe, Japan) followed by incubation with fluorescent secondary antibody (anti–rabbit IgG-Alexa Fluor).

CRISPR/Cas9 Genome Editing

The 20-nucleotide guide sequences targeting rat FGFR1 were designed using the CRISPR design tool at www.genome-engineering.org/crispr and cloned into a bicistronic expression vector (pX330) containing human codon–optimized Cas9 and the RNA components (Addgene). The guide sequence targeting exon 2 of rat FGFR1 was as follows: FGFR1 5′-GTCTGCACATCATCGCGCGAGC-3′. The single-guide RNAs in the pX330 vector (4 μg) were combined with an EGFP vector (1 μg; Clontech) and cotransfected into UMR-106 cells using FuGENE-6. Twenty-four hours post-transfection, the cells were trypsinized, washed with PBS, and resuspended in FACS buffer (PBS, 5 mM EDTA, 2% FBS, and 100 μg/ml penicillin/streptomycin). GFP-positive cells were single-cell sorted by FACS into a 96-well plate in DMEM/F-12 containing 20% FBS and 100 μg/ml penicillin/streptomycin. Single clones were expanded and screened for FGFR1 by protein immunoblotting.

Statistical Analyses

Significance between groups for quantitative PCR analyses was assessed using ANOVA analysis with a Tukey HSD *post hoc* test. Differences between serum biochemistries and RNA expression *in vitro* were assessed with paired *t* test. Significance for all tests was set at $P<0.05$, and data are presented as means ± SEM.

Disclosures

Go to:

L.M.O., M.S.C., M.B., R.L.J., J.M.W., and R.C.S. are employees of Eli Lilly and Company (Indianapolis, IN), and A.K.T. is an employee of Covance Inc. (Greenfield, IN). K.E.W. received royalties from Kyowa Hakko Kirin Co., Ltd. (Tokyo, Japan) for licensing of the *fibroblast growth factor-23* (*FGF23*) gene and the anti–FGF23 mAb clinical trials and has had research funding from Eli Lilly and Company. The other

authors declare no conflicts.

Supplementary Material

Go to:

Supplemental Data:

Acknowledgments

Go to:

The authors thank Chetan Patel and Haiyan Sun (Eli Lilly and Company) for supplying the IMC-A1 antibody, Dr. Armando Irizarry for evaluating liver histology, Dianna L. Jaqua and Zhonghua Qi for their help with the db/db-eNOS$^{-/-}$ mice, and Dr. Nati Hernando and Dr. Carsten Wagner (Institute of Physiology and Zurich Center for Integrative Human Physiology) for generously providing the anti-Npt2a antibody.

The authors acknowledge support from National Institutes of Health grants T32-HL007910 (to J.M.H.), F32-AR065389 (to E.L.C.), R01-DK063934 (to K.E.W.), and R01-DK95784 (to K.E.W.); the Indiana Genomics Initiative of Indiana University supported in part by the Lilly Endowment, Inc. (K.E.W.); and a Showalter Scholar award (to K.E.W.) supported through the Ralph W. and Grace M. Showalter Research Trust Fund.

Footnotes

Go to:

Published online ahead of print. Publication date available at www.jasn.org.

This article contains supplemental material online at http://jasn.asnjournals.org/lookup/suppl/doi:10.1681/ASN.2015111266/-/DCSupplemental.

References

Go to:

1. Fliser D, Kollerits B, Neyer U, Ankerst DP, Lhotta K, Lingenhel A, Ritz E, Kronenberg F, Kuen E, König P, Kraatz G, Mann JF, Müller GA, Köhler H, Riegler P, Riegler P.: Fibroblast growth factor 23 (FGF23) predicts progression of chronic kidney disease: The Mild to Moderate Kidney Disease (MMKD) Study. J Am Soc Nephrol 18: 2600–2608, 2007 [PubMed: 17656479]

2. Mirza MA, Larsson A, Melhus H, Lind L, Larsson TE.: Serum intact FGF23 associate with left ventricular mass, hypertrophy and geometry in an elderly population. Atherosclerosis 207: 546–551, 2009 [PubMed: 19524924]

3. Gutiérrez OM, Mannstadt M, Isakova T, Rauh-Hain JA, Tamez H, Shah A, Smith K, Lee H, Thadhani R, Jüppner H, Wolf M.: Fibroblast growth factor 23 and mortality among patients undergoing hemodialysis. N Engl J Med 359: 584–592, 2008 [PMCID: PMC2890264] [PubMed: 18687639]

4. Scialla JJ, Xie H, Rahman M, Anderson AH, Isakova T, Ojo A, Zhang X, Nessel L, Hamano T, Grunwald JE, Raj DS, Yang W, He J, Lash JP, Go AS, Kusek JW, Feldman H, Wolf M; Chronic Renal Insufficiency Cohort (CRIC) Study Investigators .: Fibroblast growth factor-23 and cardiovascular events in CKD. J Am Soc Nephrol 25: 349–360, 2014 [PMCID: PMC3904568] [PubMed: 24158986]

5. Ix JH, Katz R, Kestenbaum BR, de Boer IH, Chonchol M, Mukamal KJ, Rifkin D, Siscovick DS, Sarnak MJ, Shlipak MG.: Fibroblast growth factor-23 and death, heart failure, and cardiovascular events in community-living individuals: CHS (Cardiovascular Health Study). J Am Coll Cardiol 60: 200–207, 2012 [PMCID: PMC3396791] [PubMed: 22703926]

6. Block GA, Wheeler DC, Persky MS, Kestenbaum B, Ketteler M, Spiegel DM, Allison MA, Asplin J, Smits G, Hoofnagle AN, Kooienga L, Thadhani R, Mannstadt M, Wolf M, Chertow GM.: Effects of phosphate binders in moderate CKD. J Am Soc Nephrol 23: 1407–1415, 2012 [PMCID: PMC3402292]

[PubMed: 22822075]

7. Navaneethan SD, Palmer SC, Craig JC, Elder GJ, Strippoli GF.: Benefits and harms of phosphate binders in CKD: A systematic review of randomized controlled trials. Am J Kidney Dis 54: 619–637, 2009 [PubMed: 19692157]

8. Yokoyama K, Hirakata H, Akiba T, Fukagawa M, Nakayama M, Sawada K, Kumagai Y, Block GA.: Ferric citrate hydrate for the treatment of hyperphosphatemia in nondialysis-dependent CKD. Clin J Am Soc Nephrol 9: 543–552, 2014 [PMCID: PMC3944759] [PubMed: 24408120]

9. Farrow EG, Davis SI, Ward LM, Summers LJ, Bubbear JS, Keen R, Stamp TC, Baker LR, Bonewald LF, White KE.: Molecular analysis of DMP1 mutants causing autosomal recessive hypophosphatemic rickets. Bone 44: 287–294, 2009 [PMCID: PMC2669955] [PubMed: 19007919]

10. Liu S, Tang W, Zhou J, Stubbs JR, Luo Q, Pi M, Quarles LD.: Fibroblast growth factor 23 is a counter-regulatory phosphaturic hormone for vitamin D. J Am Soc Nephrol 17: 1305–1315, 2006 [PubMed: 16597685]

11. Shimada T, Mizutani S, Muto T, Yoneya T, Hino R, Takeda S, Takeuchi Y, Fujita T, Fukumoto S, Yamashita T.: Cloning and characterization of FGF23 as a causative factor of tumor-induced osteomalacia. Proc Natl Acad Sci USA 98: 6500–6505, 2001 [PMCID: PMC33497] [PubMed: 11344269]

12. Krajisnik T, Björklund P, Marsell R, Ljunggren O, Akerström G, Jonsson KB, Westin G, Larsson TE.: Fibroblast growth factor-23 regulates parathyroid hormone and 1alpha-hydroxylase expression in cultured bovine parathyroid cells. J Endocrinol 195: 125–131, 2007 [PubMed: 17911404]

13. Ben-Dov IZ, Galitzer H, Lavi-Moshayoff V, Goetz R, Kuro-o M, Mohammadi M, Sirkis R, Naveh-Many T, Silver J.: The parathyroid is a target organ for FGF23 in rats. J Clin Invest 117: 4003–4008, 2007 [PMCID: PMC2066196] [PubMed: 17992255]

14. Rhee Y, Bivi N, Farrow E, Lezcano V, Plotkin LI, White KE, Bellido T.: Parathyroid hormone receptor signaling in osteocytes increases the expression of fibroblast growth factor-23 in vitro and in vivo. Bone 49: 636–643, 2011 [PMCID: PMC3167030] [PubMed: 21726676]

15. Ichikawa S, Imel EA, Kreiter ML, Yu X, Mackenzie DS, Sorenson AH, Goetz R, Mohammadi M, White KE, Econs MJ.: A homozygous missense mutation in human KLOTHO causes severe tumoral calcinosis. J Musculoskelet Neuronal Interact 7: 318–319, 2007 [PubMed: 18094491]

16. Benet-Pagès A, Orlik P, Strom TM, Lorenz-Depiereux B.: An FGF23 missense mutation causes familial tumoral calcinosis with hyperphosphatemia. Hum Mol Genet 14: 385–390, 2005 [PubMed: 15590700]

17. Larsson T, Yu X, Davis SI, Draman MS, Mooney SD, Cullen MJ, White KE.: A novel recessive mutation in fibroblast growth factor-23 causes familial tumoral calcinosis. J Clin Endocrinol Metab 90: 2424–2427, 2005 [PubMed: 15687325]

18. Bergwitz C, Banerjee S, Abu-Zahra H, Kaji H, Miyauchi A, Sugimoto T, Jüppner H.: Defective O-glycosylation due to a novel homozygous S129P mutation is associated with lack of fibroblast growth factor 23 secretion and tumoral calcinosis. J Clin Endocrinol Metab 94: 4267–4274, 2009 [PMCID: PMC2775647] [PubMed: 19837926]

19. Garringer HJ, Fisher C, Larsson TE, Davis SI, Koller DL, Cullen MJ, Draman MS, Conlon N, Jain A, Fedarko NS, Dasgupta B, White KE.: The role of mutant UDP-N-acetyl-alpha-D-galactosamine-polypeptide N-acetylgalactosaminyltransferase 3 in regulating serum intact fibroblast growth factor 23 and matrix extracellular phosphoglycoprotein in heritable tumoral calcinosis. J Clin Endocrinol Metab 91:

4037–4042, 2006 [PubMed: 16868048]

20. Econs MJ, McEnery PT.: Autosomal dominant hypophosphatemic rickets/osteomalacia: Clinical characterization of a novel renal phosphate-wasting disorder. J Clin Endocrinol Metab 82: 674–681, 1997 [PubMed: 9024275]

21. Urakawa I, Yamazaki Y, Shimada T, Iijima K, Hasegawa H, Okawa K, Fujita T, Fukumoto S, Yamashita T.: Klotho converts canonical FGF receptor into a specific receptor for FGF23. Nature 444: 770–774, 2006 [PubMed: 17086194]

22. Kuro-o M, Matsumura Y, Aizawa H, Kawaguchi H, Suga T, Utsugi T, Ohyama Y, Kurabayashi M, Kaname T, Kume E, Iwasaki H, Iida A, Shiraki-Iida T, Nishikawa S, Nagai R, Nabeshima YI.: Mutation of the mouse klotho gene leads to a syndrome resembling ageing. Nature 390: 45–51, 1997 [PubMed: 9363890]

23. Hu MC, Shi M, Zhang J, Quiñones H, Griffith C, Kuro-o M, Moe OW.: Klotho deficiency causes vascular calcification in chronic kidney disease. J Am Soc Nephrol 22: 124–136, 2011 [PMCID: PMC3014041] [PubMed: 21115613]

24. Nakatani T, Sarraj B, Ohnishi M, Densmore MJ, Taguchi T, Goetz R, Mohammadi M, Lanske B, Razzaque MS.: In vivo genetic evidence for klotho-dependent, fibroblast growth factor 23 (Fgf23) -mediated regulation of systemic phosphate homeostasis. FASEB J 23: 433–441, 2009 [PMCID: PMC2630784] [PubMed: 18835926]

25. Shimada T, Kakitani M, Yamazaki Y, Hasegawa H, Takeuchi Y, Fujita T, Fukumoto S, Tomizuka K, Yamashita T.: Targeted ablation of Fgf23 demonstrates an essential physiological role of FGF23 in phosphate and vitamin D metabolism. J Clin Invest 113: 561–568, 2004 [PMCID: PMC338262] [PubMed: 14966565]

26. Zhao HJ, Wang S, Cheng H, Zhang MZ, Takahashi T, Fogo AB, Breyer MD, Harris RC.: Endothelial nitric oxide synthase deficiency produces accelerated nephropathy in diabetic mice. J Am Soc Nephrol 17: 2664–2669, 2006 [PMCID: PMC4618687] [PubMed: 16971655]

27. Mohan S, Reddick RL, Musi N, Horn DA, Yan B, Prihoda TJ, Natarajan M, Abboud-Werner SL.: Diabetic eNOS knockout mice develop distinct macro- and microvascular complications. Lab Invest 88: 515–528, 2008 [PubMed: 18391994]

28. Asai O, Nakatani K, Tanaka T, Sakan H, Imura A, Yoshimoto S, Samejima K, Yamaguchi Y, Matsui M, Akai Y, Konishi N, Iwano M, Nabeshima Y, Saito Y.: Decreased renal α-Klotho expression in early diabetic nephropathy in humans and mice and its possible role in urinary calcium excretion. Kidney Int 81: 539–547, 2012 [PubMed: 22217880]

29. Ghosh B, Brojen T, Banerjee S, Singh N, Singh S, Sharma OP, Prakash J.: The high prevalence of chronic kidney disease-mineral bone disorders: A hospital-based cross-sectional study. Indian J Nephrol 22: 285–291, 2012 [PMCID: PMC3495351] [PubMed: 23162273]

30. Imura A, Iwano A, Tohyama O, Tsuji Y, Nozaki K, Hashimoto N, Fujimori T, Nabeshima Y.: Secreted Klotho protein in sera and CSF: implication for post-translational cleavage in release of Klotho protein from cell membrane. FEBS letters 565: 143–147, 2004 [PubMed: 15135068]

31. Matsumura Y, Aizawa H, Shiraki-Iida T, Nagai R, Kuro-o M, Nabeshima Y.: Identification of the human klotho gene and its two transcripts encoding membrane and secreted klotho protein. Biochem Biophys Res Commun 242: 626–630, 1998 [PubMed: 9464267]

32. Goetz R, Nakada Y, Hu MC, Kurosu H, Wang L, Nakatani T, Shi M, Eliseenkova AV, Razzaque MS,

Moe OW, Kuro-o M, Mohammadi M.: Isolated C-terminal tail of FGF23 alleviates hypophosphatemia by inhibiting FGF23-FGFR-Klotho complex formation. Proc Natl Acad Sci USA 107: 407–412, 2010 [PMCID: PMC2806769] [PubMed: 19966287]

33. Li H, Martin A, David V, Quarles LD.: Compound deletion of Fgfr3 and Fgfr4 partially rescues the Hyp mouse phenotype. Am J Physiol Endocrinol Metab 300: E508–E517, 2011 [PMCID: PMC3064005] [PubMed: 21139072]

34. Kurosu H, Ogawa Y, Miyoshi M, Yamamoto M, Nandi A, Rosenblatt KP, Baum MG, Schiavi S, Hu MC, Moe OW, Kuro-o M.: Regulation of fibroblast growth factor-23 signaling by klotho. J Biol Chem 281: 6120–6123, 2006 [PMCID: PMC2637204] [PubMed: 16436388]

35. Olauson H, Lindberg K, Amin R, Jia T, Wernerson A, Andersson G, Larsson TE.: Targeted deletion of Klotho in kidney distal tubule disrupts mineral metabolism. J Am Soc Nephrol 23: 1641–1651, 2012 [PMCID: PMC3458458] [PubMed: 22878961]

36. Hu MC, Shi M, Zhang J, Pastor J, Nakatani T, Lanske B, Razzaque MS, Rosenblatt KP, Baum MG, Kuro-o M, Moe OW.: Klotho: A novel phosphaturic substance acting as an autocrine enzyme in the renal proximal tubule. FASEB J 24: 3438–3450, 2010 [PMCID: PMC2923354] [PubMed: 20466874]

37. Wang Y, Sun Z.: Klotho gene delivery prevents the progression of spontaneous hypertension and renal damage. Hypertension 54: 810–817, 2009 [PMCID: PMC2814175] [PubMed: 19635988]

38. Satoh M, Nagasu H, Morita Y, Yamaguchi TP, Kanwar YS, Kashihara N.: Klotho protects against mouse renal fibrosis by inhibiting Wnt signaling. Am J Physiol Renal Physiol 303: F1641–F1651, 2012 [PMCID: PMC3532475] [PubMed: 23034937]

39. Smith RC, O'Bryan LM, Farrow EG, Summers LJ, Clinkenbeard EL, Roberts JL, Cass TA, Saha J, Broderick C, Ma YL, Zeng QQ, Kharitonenkov A, Wilson JM, Guo Q, Sun H, Allen MR, Burr DB, Breyer MD, White KE.: Circulating αKlotho influences phosphate handling by controlling FGF23 production. J Clin Invest 122: 4710–4715, 2012 [PMCID: PMC3533557] [PubMed: 23187128]

40. Brownstein CA, Adler F, Nelson-Williams C, Iijima J, Li P, Imura A, Nabeshima Y, Reyes-Mugica M, Carpenter TO, Lifton RP.: A translocation causing increased alpha-klotho level results in hypophosphatemic rickets and hyperparathyroidism. Proc Natl Acad Sci USA 105: 3455–3460, 2008 [PMCID: PMC2265125] [PubMed: 18308935]

41. Felaco M, Grilli A, De Lutiis MA, Patruno A, Libertini N, Taccardi AA, Di Napoli P, Di Giulio C, Barbacane R, Conti P.: Endothelial nitric oxide synthase (eNOS) expression and localization in healthy and diabetic rat hearts. Ann Clin Lab Sci 31: 179–186, 2001 [PubMed: 11337908]

42. Nakagawa T, Sato W, Glushakova O, Heinig M, Clarke T, Campbell-Thompson M, Yuzawa Y, Atkinson MA, Johnson RJ, Croker B.: Diabetic endothelial nitric oxide synthase knockout mice develop advanced diabetic nephropathy. J Am Soc Nephrol 18: 539–550, 2007 [PubMed: 17202420]

43. Yuen DA, Stead BE, Zhang Y, White KE, Kabir MG, Thai K, Advani SL, Connelly KA, Takano T, Zhu L, Cox AJ, Kelly DJ, Gibson IW, Takahashi T, Harris RC, Advani A.: eNOS deficiency predisposes podocytes to injury in diabetes. J Am Soc Nephrol 23: 1810–1823, 2012 [PMCID: PMC3482727] [PubMed: 22997257]

44. Tervaert TW, Mooyaart AL, Amann K, Cohen AH, Cook HT, Drachenberg CB, Ferrario F, Fogo AB, Haas M, de Heer E, Joh K, Noël LH, Radhakrishnan J, Seshan SV, Bajema IM, Bruijn JA; Renal Pathology Society .: Pathologic classification of diabetic nephropathy. J Am Soc Nephrol 21: 556–563, 2010 [PubMed: 20167701]

45. Fioretto P, Mauer M.: Histopathology of diabetic nephropathy. Semin Nephrol 27: 195–207, 2007 [PMCID: PMC2746982] [PubMed: 17418688]

46. Sun N, Zou H, Yang L, Morita K, Gong P, Shiba T, Akagawa Y, Yuan Q.: Inorganic polyphosphates stimulate FGF23 expression through the FGFR pathway. Biochem Biophys Res Commun 428: 298–302, 2012 [PubMed: 23085229]

47. Goetz R, Beenken A, Ibrahimi OA, Kalinina J, Olsen SK, Eliseenkova AV, Xu C, Neubert TA, Zhang F, Linhardt RJ, Yu X, White KE, Inagaki T, Kliewer SA, Yamamoto M, Kurosu H, Ogawa Y, Kuro-o M, Lanske B, Razzaque MS, Mohammadi M.: Molecular insights into the klotho-dependent, endocrine mode of action of fibroblast growth factor 19 subfamily members. Mol Cell Biol 27: 3417–3428, 2007 [PMCID: PMC1899957] [PubMed: 17339340]

48. Sun HD, Malabunga M, Tonra JR, DiRenzo R, Carrick FE, Zheng H, Berthoud HR, McGuinness OP, Shen J, Bohlen P, Leibel RL, Kussie P.: Monoclonal antibody antagonists of hypothalamic FGFR1 cause potent but reversible hypophagia and weight loss in rodents and monkeys. Am J Physiol Endocrinol Metab 292: E964–E976, 2007 [PubMed: 17132826]

49. Fang Y, Ginsberg C, Sugatani T, Monier-Faugere MC, Malluche H, Hruska KA.: Early chronic kidney disease-mineral bone disorder stimulates vascular calcification. Kidney Int 85: 142–150, 2014 [PMCID: PMC3836911] [PubMed: 23884339]

50. Mizobuchi M, Towler D, Slatopolsky E.: Vascular calcification: The killer of patients with chronic kidney disease. J Am Soc Nephrol 20: 1453–1464, 2009 [PubMed: 19478096]

51. Leibrock CB, Alesutan I, Voelkl J, Pakladok T, Michael D, Schleicher E, Kamyabi-Moghaddam Z, Quintanilla-Martinez L, Kuro OM, Lang F.: NH4Cl treatment prevents tissue calcification in Klotho deficiency. J Am Soc Nephrol 26: 2423–2433, 2015 [PMCID: PMC4587682] [PubMed: 25644113]

52. Leibrock CB, Alesutan I, Voelkl J, Michael D, Castor T, Kohlhofer U, Quintanilla-Martinez L, Kubler L, Mannheim JG, Pichler BJ, Rosenblatt KP, Kuro OM, Lang F.: Acetazolamide sensitive tissue calcification and aging of klotho-hypomorphic mice. J Mol Med 94: 95–106, 2015 [PubMed: 26307633]

53. Olauson H, Lindberg K, Amin R, Sato T, Jia T, Goetz R, Mohammadi M, Andersson G, Lanske B, Larsson TE.: Parathyroid-specific deletion of Klotho unravels a novel calcineurin-dependent FGF23 signaling pathway that regulates PTH secretion. PLoS Genet 9: e1003975, 2013 [PMCID: PMC3861040] [PubMed: 24348262]

54. Aizawa H, Saito Y, Nakamura T, Inoue M, Imanari T, Ohyama Y, Matsumura Y, Masuda H, Oba S, Mise N, Kimura K, Hasegawa A, Kurabayashi M, Kuro-o M, Nabeshima Y, Nagai R.: Downregulation of the Klotho gene in the kidney under sustained circulatory stress in rats. Biochem Biophys Res Commun 249: 865–871, 1998 [PubMed: 9731228]

55. Koh N, Fujimori T, Nishiguchi S, Tamori A, Shiomi S, Nakatani T, Sugimura K, Kishimoto T, Kinoshita S, Kuroki T, Nabeshima Y.: Severely reduced production of klotho in human chronic renal failure kidney. Biochem Biophys Res Commun 280: 1015–1020, 2001 [PubMed: 11162628]

56. Moe SM, Radcliffe JS, White KE, Gattone VH 2nd, Seifert MF, Chen X, Aldridge B, Chen NX.: The pathophysiology of early-stage chronic kidney disease-mineral bone disorder (CKD-MBD) and response to phosphate binders in the rat. J Bone Miner Res 26: 2672–2681, 2011 [PubMed: 21826734]

57. London GM, Guérin AP, Marchais SJ, Métivier F, Pannier B, Adda H.: Arterial media calcification in end-stage renal disease: Impact on all-cause and cardiovascular mortality. Nephrol Dial Transplant 18: 1731–1740, 2003 [PubMed: 12937218]

58. Sigrist MK, Taal MW, Bungay P, McIntyre CW.: Progressive vascular calcification over 2 years is associated with arterial stiffening and increased mortality in patients with stages 4 and 5 chronic kidney disease. Clin J Am Soc Nephrol 2: 1241–1248, 2007 [PubMed: 17928470]

59. Goodman WG, Goldin J, Kuizon BD, Yoon C, Gales B, Sider D, Wang Y, Chung J, Emerick A, Greaser L, Elashoff RM, Salusky IB.: Coronary-artery calcification in young adults with end-stage renal disease who are undergoing dialysis. N Engl J Med 342: 1478–1483, 2000 [PubMed: 10816185]

60. Xiao Z, Huang J, Cao L, Liang Y, Han X, Quarles LD.: Osteocyte-specific deletion of Fgfr1 suppresses FGF23. PLoS One 9: e104154, 2014 [PMCID: PMC4121311] [PubMed: 25089825]

61. Wu AL, Feng B, Chen MZ, Kolumam G, Zavala-Solorio J, Wyatt SK, Gandham VD, Carano RA, Sonoda J.: Antibody-mediated activation of FGFR1 induces FGF23 production and hypophosphatemia. PLoS One 8: e57322, 2013 [PMCID: PMC3579827] [PubMed: 23451204]

62. White KE, Cabral JM, Davis SI, Fishburn T, Evans WE, Ichikawa S, Fields J, Yu X, Shaw NJ, McLellan NJ, McKeown C, Fitzpatrick D, Yu K, Ornitz DM, Econs MJ.: Mutations that cause osteoglophonic dysplasia define novel roles for FGFR1 in bone elongation. Am J Hum Genet 76: 361–367, 2005 [PMCID: PMC1196382] [PubMed: 15625620]

63. Harlan SM, Ostroski RA, Coskun T, Yantis LD, Breyer MD, Heuer JG.: Viral transduction of renin rapidly establishes persistent hypertension in diverse murine strains. Am J Physiol Regul Integr Comp Physiol 309: R467–R474, 2015 [PubMed: 26108870]

64. Farrow EG, Yu X, Summers LJ, Davis SI, Fleet JC, Allen MR, Robling AG, Stayrook KR, Jideonwo V, Magers MJ, Garringer HJ, Vidal R, Chan RJ, Goodwin CB, Hui SL, Peacock M, White KE.: Iron deficiency drives an autosomal dominant hypophosphatemic rickets (ADHR) phenotype in fibroblast growth factor-23 (Fgf23) knock-in mice. Proc Natl Acad Sci USA 108: E1146–E1155, 2011 [PMCID: PMC3219119] [PubMed: 22006328]

65. Livak KJ, Schmittgen TD.: Analysis of relative gene expression data using real-time quantitative PCR and the 2(-Delta Delta C(T)) Method. Methods 25: 402–408, 2001 [PubMed: 11846609]

66. Virkki LV, Forster IC, Hernando N, Biber J, Murer H.: Functional characterization of two naturally occurring mutations in the human sodium-phosphate cotransporter type IIa. J Bone Miner Res 18: 2135–2141, 2003 [PubMed: 14672348]

Figures and Tables

Go to:

Figure 1.

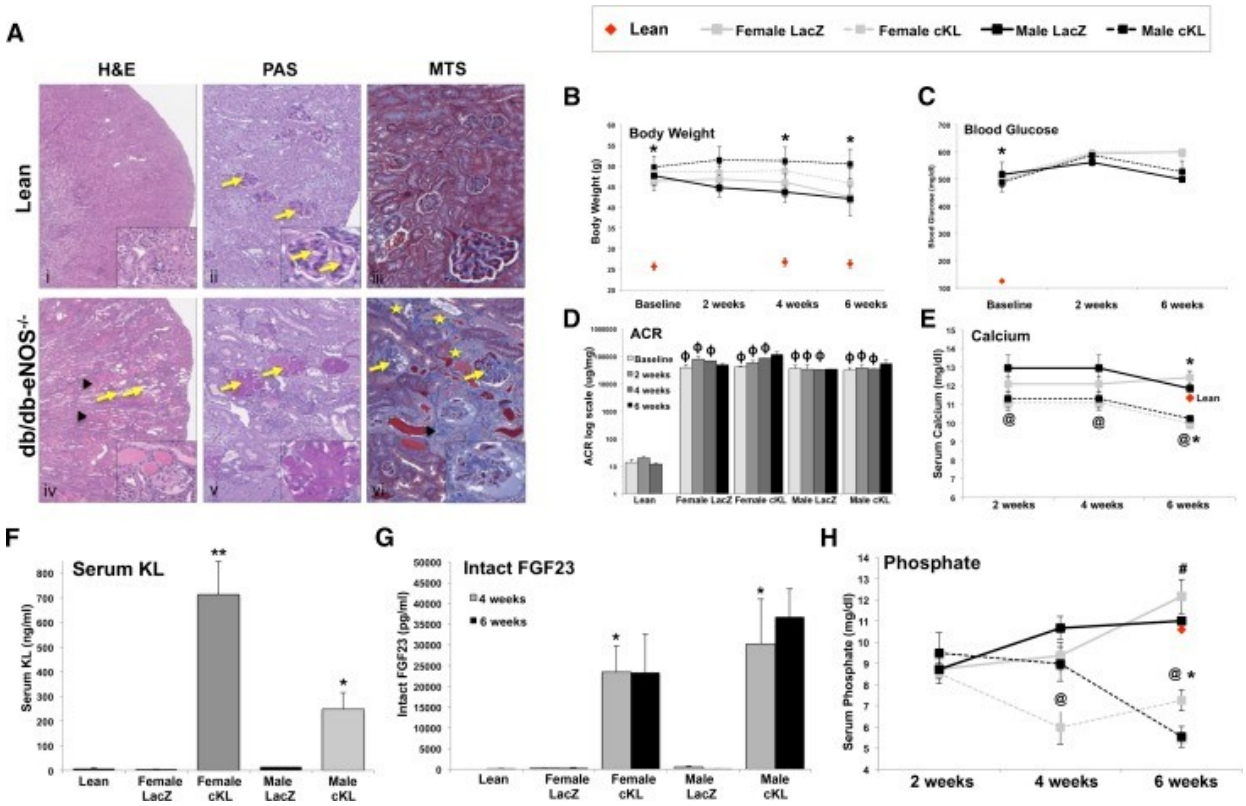

cKL rescues hyperphosphatemia in a model of diabetic renal failure. (A) Representative differences in histopathologic changes as shown by three staining methods, H&E, periodic acid–Schiff (PAS), and Masson trichrome (MTS), in kidneys from (i–iii) control lean (db/dm) mice and (iv–vi) db/db-eNOS$^{-/-}$ LacZ mice. There is prominent presence of tubular protein (arrowheads and inset in iv) and dilated tubules (arrows in iv) in the H&E-stained sections from db/db-eNOS$^{-/-}$ LacZ mice that was absent in control lean mice (inset i). In db/db-eNOS$^{-/-}$ LacZ mice there was notable mesangial matrix deposition highlighted by PAS staining (arrows and inset v) that obliterates normal capillary loops and cellularity in the glomeruli found in control lean mice (arrows and inset ii). Marked interstitial fibrosis highlighted in blue by the MTS stain (stars in vi) and prominent glomerular fibrosis (arrows and inset in vi) with occasional glomerular sclerosis (arrow head in vi) in db/db-eNOS$^{-/-}$ LacZ mice and absent in control lean mice (inset iii). (B) Male and female body weights (grams) from baseline and 2, 4, and 6 weeks post-treatment. All db/db-eNOS$^{-/-}$ mice, regardless of treatment, were significantly heavier than age–matched lean control mice. *P<0.01. (C) Blood glucose was elevated above baseline lean controls in male and female db/db-eNOS$^{-/-}$ mice, regardless of treatment. *P<0.01. (D) Urine ACR was significantly elevated in male and female db/db-eNOS$^{-/-}$ mice compared with age–matched lean controls. $^{\phi}P$<0.001. (E) Serum calcium was reduced in AAV-cKL–treated female db/db-eNOS$^{-/-}$ mice at 2, 4, and 6 weeks postinjection compared with AAV-LacZ–treated female db/db-eNOS$^{-/-}$ mice and age–matched lean controls. By 6 weeks, serum calcium had significantly risen in AAV-LacZ female db/db-eNOS$^{-/-}$ mice compared with lean controls. *P<0.05 (age–matched lean controls); $^{@}P$<0.05 (AAV-LacZ–treated female db/db-eNOS$^{-/-}$ mice). (F) Serum Klotho levels in db/db-eNOS$^{-/-}$ male and female mice were significantly increased with AAV-cKL treatment 6 weeks postinjection. *P<0.05 versus all AAV-LacZ and lean mice; **P<0.01 versus all AAV-LacZ and lean mice. (G) Intact FGF23 was significantly elevated in db/db-eNOS$^{-/-}$ male and female mice with AAV-cKL treatment 4 weeks postinjection and remained elevated at 6 weeks. *P<0.05. (H) Serum phosphate was significantly reduced in female db/db-eNOS$^{-/-}$ mice by 4 and 6 weeks post–AAV-cKL injection compared with female db/db-eNOS$^{-/-}$ mice injected with AAV-LacZ and lean controls. Female db/db-eNOS$^{-/-}$ mice treated with AAV-LacZ had significantly elevated serum phosphate by 6 weeks after treatment. *P<0.05 (lean controls); $^{@}P$<0.05 (AAV-LacZ mice); $^{\#}P$<0.05 versus 2 and 4 weeks.

Figure 2.

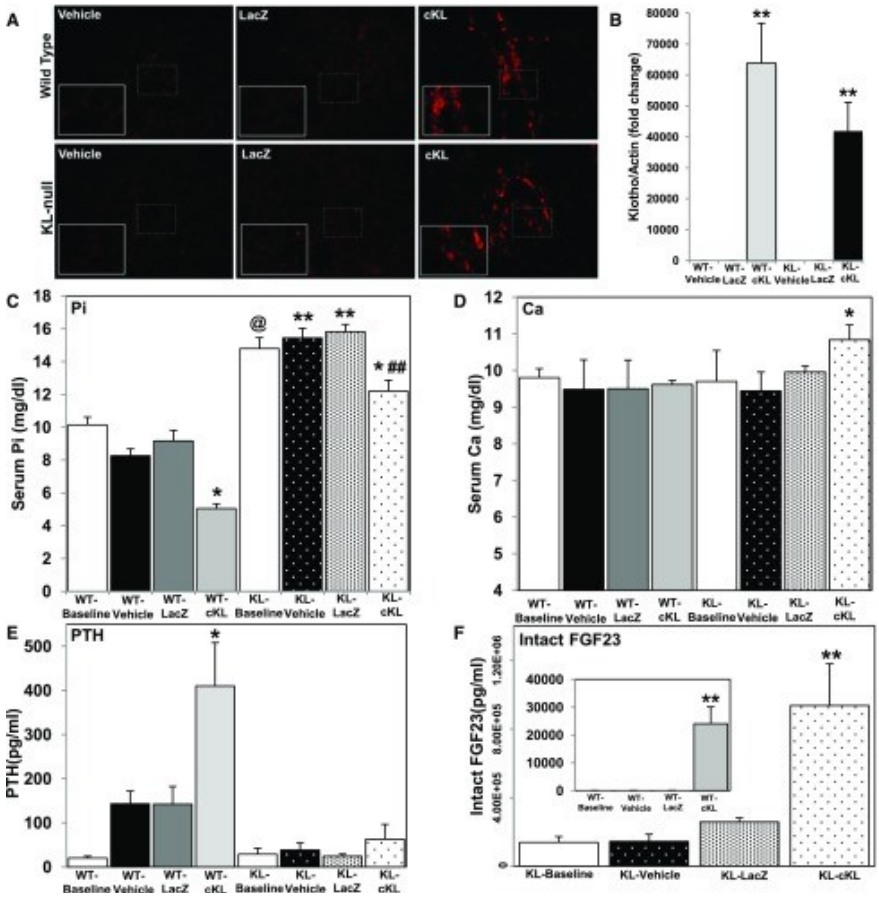

Biochemical and endocrine effects of AAV-cKL in WT and Klotho-null mice. (A) Liver sections from WT and α*KL*-null mice were examined for *α*KL expression by immunofluorescence staining. *α*KL protein was only observed in mice delivered AAV-cKL, and staining (red) localized to cells near hepatic portal venules. (B) WT and α*KL*-null livers were assessed for cKL mRNA expression. WT mice and α*KL*-null mice treated with AAV-cKL had highly expressed cKL mRNA (approximately 60,000- and 40,000-fold increases, respectively). There was no significant difference between AAV-cKL–treated mice. $^{**}P<0.01$. (C) α*KL*-null mice were hyperphosphatemic compared with WT mice at baseline and across treatment groups. Compared with like genotype controls (vehicle or LacZ), serum phosphate (Pi) was reduced in WT and Klotho mice treated with cKL. $^{*}P<0.01$; $^{**}P<0.001$ (across treatment groups); $^{\#\#}P<0.01$ (across treatment groups); $^{@}P<0.001$ (baseline). (D) Within genotypic groups, serum calcium (Ca) was unaffected by 4 weeks of cKL treatment. However, a slight elevation in serum calcium in Klotho-cKL was significant compared with WT-cKL. $^{*}P<0.05$ versus WT-cKL. (E) cKL induced hyperparathyroidism in WT mice, but Klotho mice exhibited sustained hypoparathyroidism, regardless of treatment. $^{*}P<0.05$. (F, inset) Intact FGF23 was significantly increased in WT mice treated with cKL. $^{**}P<0.01$ versus baseline, vehicle, and AAV-LacZ. (F) KL mice had baseline elevated intact FGF23 versus WT mice at baseline and displayed a further increase with cKL treatment. $^{**}P<0.01$ versus vehicle and LacZ; $^{@}P<0.05$ (baseline).

Figure 3.

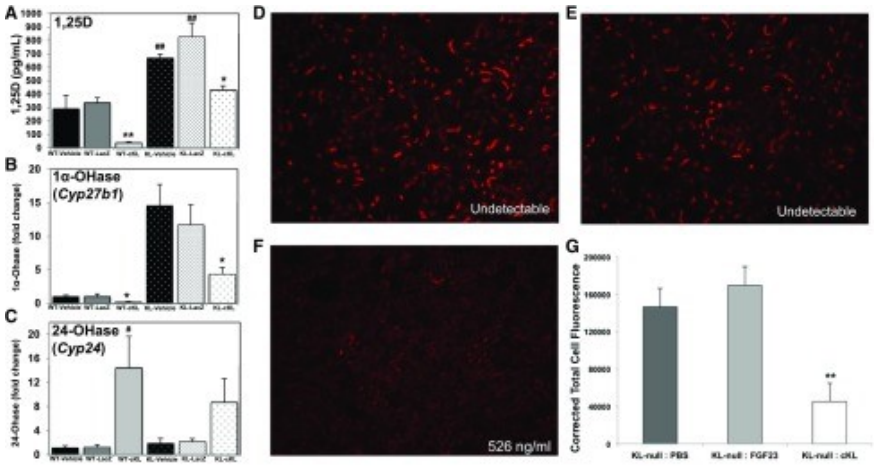

cKL influences renal gene expression. (A) Serum 1,25D concentrations were tested in WT and α*KL*-null mice after 4 weeks of treatment. Sustained delivery of AAV-cKL in WT mice reduced 1,25D. α*KL*-null mice exhibit elevated 1,25D; AAV-cKL reduced 1,25D. **P*<0.05; ***P*<0.01; $^{\#\#}P$<0.01. (B) Delivery of AAV-cKL reduced renal expression of 1*α*-OHase (*Cyp27b1*) in both WT and α*KL*-null mice. **P*<0.05. (C) Renal expression of 24-OHase (*Cyp24a1*) was increased in WT-cKL mice, whereas in KL-cKL mice, there was a trend for 24-OHase elevation, which was not statistically significant. $^{\#}P$<0.05. (D) α*KL*-null mice were injected intravenously with PBS, FGF23 (1 *μ*g/g body wt), or cKL (1 *μ*g/g body wt) for 1 hour and then, analyzed for kidney Npt2a expression by immunofluorescence. (D) Vehicle (cKL undetectable) and (E) FGF23-injected mice (cKL undetectable) had similar levels of Npt2a. (F) After injection with cKL, Npt2a expression was reduced. The concentration represents the serum cKL levels after injection, assuring cKL delivery (cKL range =214–526 ng/ml). (G) Quantitative analysis showed a significant reduction of Npt2a expression in mice treated with cKL versus controls. ***P*<0.01.

Figure 4.

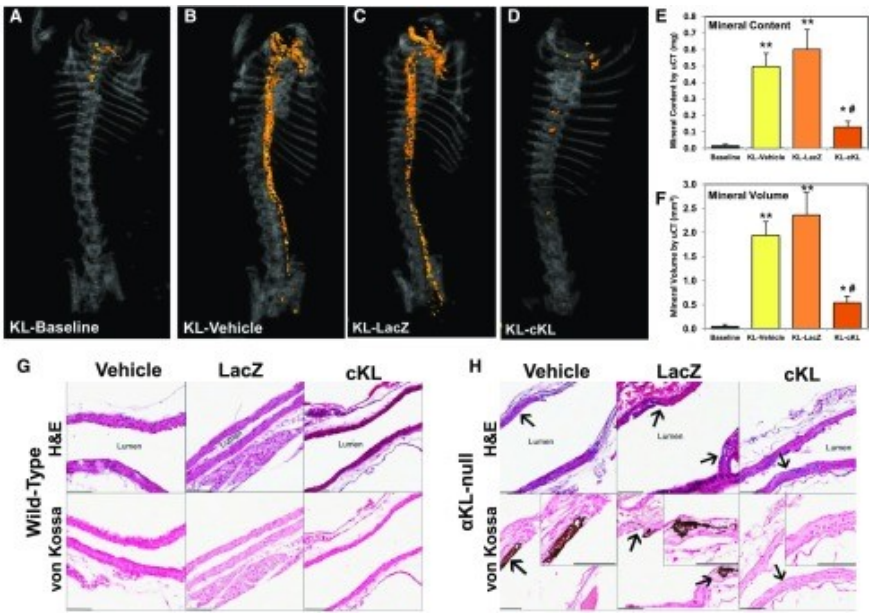

cKL prevents aortic calcification. (A) Representative μCT images of aortic calcification (orange) from Klotho mice from baseline (4 weeks of age) as well as (B) vehicle, (C) LacZ, and (D) cKL groups (treated from 4 weeks of age for 4 additional weeks). cKL administration was associated with a visually marked reduction in aortic mineralization versus Klotho-vehicle and Klotho-LacZ. (E) Mineral content and (F) mineral volume of whole aortas were quantified and determined to be significantly elevated versus all groups; however, in cKL-treated mice, mineral content and volume were significantly reduced versus Klotho-vehicle and Klotho-LacZ. Longitudinal sections of aorta from treated mice were examined by histology. *P<0.05 versus baseline; **P<0.01 versus baseline; $^{\#}P$<0.01 versus vehicle and AAV-LacZ treated. (G) Compared with WT mice, (H) α*KL*-null mice showed multifocal disruption or expansion of the aortic elastic lamina (arrows). α*KL*-null mice aortas from vehicle and AAV-LacZ–treated mice were positively stained with von Kossa (dark patches are indicative of mineralization), but <50% of such lesions from mice administered cKL stained positive (insets). Scale bar, 100 μm.

Figure 5.

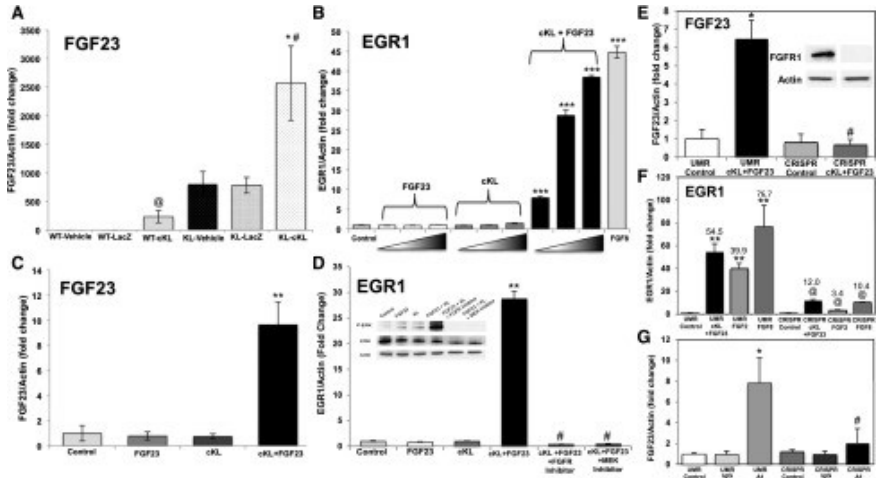

cKL signals in bone cells via FGFR1. (A) FGF23 mRNA was increased in femurs of WT mice treated with AAV-cKL. α*KL*-null mice had elevated bone FGF23 expression compared with WT mice, which was further increased in α*KL*-null mice treated with AAV-cKL. **P*<0.01 versus same genotype controls; $^{\#}$*P*<0.01 versus WT mice; $^{@}$*P*<0.01 versus controls. (B) UMR-106 cells treated with cKL or FGF23 alone showed no effects; however, a combination of cKL + FGF23 increased expression of EGR1 mRNA. The positive control FGF8 increased EGR1 mRNA. ****P*<0.001 versus control (untreated). (C) FGF23 mRNA was significantly increased in UMR-106 cells administered cKL + FGF23. ***P*<0.01 versus all other treatments. (D) EGR1 mRNA increased in response to cKL + FGF23 and was dependent on functional FGFR signaling and MEK activity, because pretreatment with either an FGFR or MEK inhibitor blocked EGR1 mRNA production as well as p-ERK expression by immunoblot (inset). ***P*<0.01 versus control and FGF23 or cKL alone; $^{\#}$*P*<0.001 versus cKL + FGF23. (E) A novel UMR-106 cell line with deletion of FGFR1 was generated *via* CRISPR-Cas. Immunoblots of lysates from the parent UMR-106 line (UMR) and the CRISPR-targeted line (CRISPR) assured ablated FGFR1 protein (inset). cKL + FGF23 increased FGF23 mRNA expression in the UMR cells, but FGF23 expression was not different from UMR control in the CRISPR line. *P* value was not significant versus UMR control. **P*<0.05 versus UMR control (untreated); $^{\#}$*P*<0.001 versus UMR cKL + FGF23. (F) EGR1 mRNA expression was increased in response to FGF2, FGF8, and cKL + FGF23 in UMR cells. This response was significantly blunted in the CRISPR cells. ***P*<0.001 versus UMR control; $^{@}$*P*<0.05 versus UMR respective treatment. (G) Administration of an FGFR1c agonist antibody increased FGF23 mRNA expression in the parent UMR cells but failed to upregulate FGF23 in CRISPR cells. **P*<0.05 versus UMR control; $^{\#}$*P*<0.05 versus UMR A1.

Articles from Journal of the American Society of Nephrology : JASN are provided here courtesy of **American Society of Nephrology**